Journal of Colloid and Interface Science 512 (2018) 730–739

Contents lists available at ScienceDirect

Journal of Colloid and Interface Science

journal homepage: www.elsevier.com/locate/jcis

Regular Article

Selective adsorption activities toward organic dyes and antibacterial performance of silver-based coordination polymers

Ang Liu, Chong-Chen Wang *, Chang-zheng Wang, Hui-fen Fu, Wang Peng, Ya-Li Cao, Hong-Yu Chu, Ao-Fei Du

Beijing Key Laboratory of Functional Materials for Building Structure and Environment Remediation/Sino-Dutch R&D Centre for Future Wastewater Treatment Technologies, Beijing University of Civil Engineering and Architecture, Beijing 100044, China

GRAPHICAL ABSTRACT

Silver-based coordination polymers were used to conduct efficiently selective uptake of organic dyes with —NH_2 & —SO_3^-. The controlled slow-release of Ag^+ ions from silver-based CPs leads to excellent antibacterial activities towards bacteria.

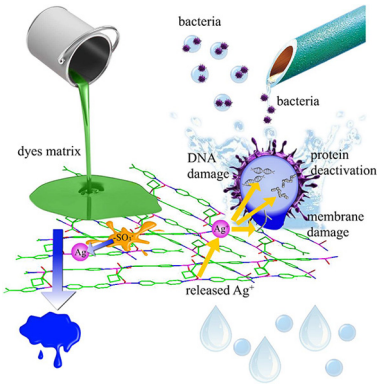

ARTICLE INFO

Article history:
Received 12 September 2017
Revised 24 October 2017
Accepted 25 October 2017
Available online 27 October 2017

Keywords:
Silver-based coordination polymer
Adsorption
Organic dyes
Adsorption mechanism
Antibacterial

ABSTRACT

Two silver-based coordination polymers, $[Ag_2(bpy)_2(cbda)]$ (**BUC-51**) and $[Ag_3(bpy)_3(cpda)]\cdot(NO_3)\cdot 9H_2O$ (**BUC-52**), have been successfully prepared by slow evaporation at room temperature. These coordination polymers exhibited good adsorptive performances toward series organic dyes with sulfonic groups, which could be ascribed to the Ag*cdots*O interaction between the silver(I) atoms in CPs and the oxygen atoms from sulfonic groups attached to organic dyes. Both **BUC-51** and **BUC-52** favoured slow release of Ag^+ ions resulting into outstanding long-term antibacterial abilities toward Gram-negative bacteria, *Escherichia coli* (*E. coli*), which was tested by a minimal inhibition concentration (MIC) benchmark and an inhibition zone testing method. Both scanning electron microscope (SEM) and transmission electron microscope (TEM) images demonstrated that these two Ag-based coordination polymers could destroy the bacterial membrane and further cause death. Additionally, the excellent stability in common solvents and good optical stability under UV–visible light facilitated their adsorptive and antibacterial applications.

* Corresponding author.
E-mail address: chongchenwang@126.com (C.-C. Wang).

https://doi.org/10.1016/j.jcis.2017.10.099
0021-9797/

1. Introduction

Coordination polymers (CPs), as a new class of inorganic-organic hybrid materials, have great potential for wide range of applications like catalysis [1,2], anti-microbial [3], gas storage and separation [4], pollutants adsorption [5], sensing [6], fluorescence [7], magnetism [8], drug delivery [9], and so on [10,11], due to their diverse compositions, easily tailored structures, ultra-high surfaces and active sites [12]. Especially, CPs are promising absorbents for high-performance adsorptive removal of pollutants from aquoues solution resulting from their striking characteristics of cavities with regular size and shape, well-defined channels, surface charge, along with excellent stability [13,14]. Furthermore, some CPs were used to selectively adsorb and efficiently separate organic pollutants with different charges from their matrix due to the electronic interactions and/or guest-guest exchange interactions [15,16]. For instance, Wang and co-workers presented chemically stable graphene-like CP, which could achieve both high-performance adsorption toward anionic organic dyes such as congo red (CR) with adsorption capacity of 4923 mg/g and efficient separation of organic dyes with different charges from their matrix [17]. CPs also exhibited outstanding antibacterial activities with high durability, considering that they could be utilized as reservoirs to slowly release metal ions such as Ag^+, Zn^{2+}, Cu^{2+} or Cu^+ with the aid of organic ligands [3,18]. It was worthy to note that Ag^+ ions could be easily diffused into a bacterial membrane and further destroy cell membrane proteins [18,19]. From this point, it is important and necessary to design and prepare Ag-based CPs as excellent antibacterial agent candidates.

In this work, two new coordination polymers, $[Ag_2(bpy)_2(cbda)]$ (**BUC-51**) and $[Ag_3(bpy)_3(cpda)]\cdot(NO_3)\cdot 9H_2O$ (**BUC-52**) were synthesized from the reaction of 4,4′-bipyridine (bpy), 1,1-cyclopropanedicarboxylic acid (H_2cpda)/1,1-cyclobutane dicarboxylic acid (H_2cbda) via slow evaporation, and were characterized by TGA, XRD and FTIR. Their adsorptive performances toward different organic dyes and antibacterial activities along with the corresponding mechanisms were investigated.

2. Experimental

2.1. Materials and methods

All GR chemicals and solvents were commercially available from J&K Chemical Ltd. and used without any further purification. *Escherichia coli* (CICC 23429) were purchased from the China Centre of Industrial Culture Collection (Beijing, China). Elemental analyses of C, H and N of the CPs were performed on Elementar Vario EL-III instrument. FTIR spectra in the region of 4000–400 cm^{-1} were recorded on a Nicolet 6700 FTIR spectrophotometer with KBr pellets. Thermogravimetric analyses were performed from 90 °C to 800 °C in air stream at a heating rate of 10 °C min^{-1} on a DTU-3c thermal analyser using α-Al_2O_3 as reference. Powder X-ray diffraction patterns were recorded using a Dandonghaoyuan DX-2700B diffractometer with Cu Kα radiation. X-ray photoelectron spectra measurement was conducted with Thermo ESCALAB 250XI. The elemental mapping was obtained on a Hitachi SU8020 scanning electron microscope. The change of bacteria was observed with the aid of microscope with Axio Imager A^2. The release rate of Ag^+ ions was tested on iCAP 7000 inductively coupled plasma optical emission spectrometer. The surface morphologies of samples were observed by JEOL-6360LV scanning electron microscope. The morphological changes of the bacteria were observed by Hitachi-HT7700 transmission electron microscopy operated at 20 kV.

2.2. Synthesis

2.2.1. $[Ag_2(bpy)_2(cbda)]$ (BUC-51)

An ammonia solution (125 mL, 0.5 mol/L) containing $AgNO_3$ (1.25 mmol, 0.21 g) and 1,1-cyclobutane dicarboxylic acid (H_2cbda, 1.25 mmol, 0.18 g) was added dropwise to an EtOH solution (125 mL) of 4,4′-bipyridine (bpy, 1.25 mmol, 0.20 g), and the mixture was stirred for 15 min, then allowed to evaporate slowly at room temperature in the dark. Block-like white crystals of $[Ag_2(bpy)_2(cbda)]$ (1) were obtained after 2 weeks (yield 90% based on $AgNO_3$). Anal. Calcd. for $C_{26}H_{22}Ag_2N_4O_4$ (%): C, 46.6; H, 3.3; N, 8.4. Found: C, 46.6; H, 3.4; N, 8.5. IR (KBr)/cm^{-1}: 3418, 1598, 1527, 1488, 1410, 1384, 1226, 1070, 805, 732, 621, 564, 510.

2.2.2. $[Ag_3(bpy)_3(cpda)]\cdot(NO_3)\cdot 9H_2O$ (BUC-52)

The synthesis of block-like white crystals of $[Ag_3(bpy)_3(cpda)]\cdot(NO_3)\cdot 9H_2O$ (**BUC-52**) followed the same procedure as for **BUC-51** except that H_2cbda was replaced with H_2cpda (yield 88% based on $AgNO_3$). Anal. Calcd. for $C_{35}H_{46}Ag_3N_7O_{16}$ (%): C, 36.7; H, 4.0; N, 8.6. Found: C, 36.8; H, 4.0; N, 8.7. IR (KBr)/cm^{-1}: 3396, 1600, 1532, 1488, 1417, 1383, 1222, 1064, 805, 727, 617, 565, 507.

2.3. Adsorption experiments

Anionic methyl orange (MO), anionic congo red (CR), cationic methylene blue (MB) and cationic rhodamine B (RhB) were selected as model pollutants to evaluate the adsorption performance of **BUC-51** and **BUC-52**. A solid sample powder (50 mg) of **BUC-51** and **BUC-52** were added to 200 mL of MO (10 mg/L), CR (50 mg/L), MB (10 mg/L) and RhB (10 mg/L) aqueous solution in a 300 mL breaker, respectively. The mixtures were vibrated in water bath shaker with speed of 150 r/min at 293 K. 1 mL aliquots were extracted using a 0.45 μm syringe filter (Tianjin Jinteng) at regular intervals for analysis. A Laspec Alpha-1860 spectrometer was used to monitor the MO, CR, MB and RhB concentration changes by the maximum absorbance at 463, 493, 664 and 552 nm, respectively.

2.4. Antibacterial activities

The antibacterial performances of **BUC-51** and **BUC-52** were used tested by agar plate diffusion assay method agar plate diffusion assay suggested by the National Committee for Clinical Laboratory Standards [20,21]. Surface water collected from Minghu Lake in BUCEA was used to investigate the antibacterial properties of **BUC-51** and **BUC-52**. Two micrograms of **BUC-51** and **BUC-52** were added to 200 mL lake water, and the control experiment was conducted at the same time without **BUC-51** and **BUC-52**. After 4 h cultivation, the supernatant was vaccinated onto Agar plate to observe the growth status of bacterial colony. Meanwhile, antibacterial activities of these two CPs were tested against *Escherichia coli* (CICC 23429) by determining the minimal inhibitory concentration (MIC), growth inhibition assay and zone of inhibition technique. All bacterial routine handlings were conducted with Luria Bertani (LB) broth at 37 °C, and long-term storage was performed in glycerol stocks stored at −30 °C. The medium was made up by dissolving agar and LB broth in distilled water.

2.4.1. Minimum inhibitory concentration (MIC)

Bacteria were placed in general LB liquid media and were agitated at 37 °C overnight. Diluted overnight bacterial and LB liquid cultures were treated with serial dilutions of **BUC-51** and **BUC-52** for 24 h while shaking at 37 °C, respectively. The MIC values were determined by the optical density measured at 600 nm (OD_{600}, Fig. S1).

2.4.2. Growth inhibition assay

Diluted bacteria and LB liquid cultures were treated with different amounts of **BUC-51** and **BUC-52** for 48 h while shaking at 37 °C, respectively. OD_{600} was measured via a UV–vis spectrometer at fixed time interval to draw the growth curves of bacteria. The growth curves of *E. coli* without CPs were also measured as blank. All the data for OD_{600} were the average values of three parallel tests.

2.4.3. Zone of inhibition technique

The mixture of dissolved agar and LB broth was autoclaved at 121 °C for 15 min and then dispensed into sterilized Petri dishes, which was allowed to solidify and then used for inoculation. The target microorganism cultures were prepared separately in 100 mL liquid LB broth medium for activation. Activated strain (50 μL) was placed onto the surface of an agar plate, and speeded evenly over the surface by means of a sterile bent glass rod. Then the neutral filters (diameter of 6 mm) infiltrating the CPs solution were put into each plate. The diameters of inhibition zones were measured by Vernier calipers, and the data were the average values of two parallel tests.

2.5. Direct method of quantification of silver release

The powders of **BUC-51** and **BUC-52** were immersed in distilled water in 250 ppm for 5 d. The released Ag^+ concentrations in the supernatant liquor were determined by ICP-OES every 4 h in the first day. After that, the released Ag^+ concentrations were measured once a day.

3. Results and discussion

3.1. Structure descriptions of BUC-51 and BUC-52

$[Ag_2(bpy)_2(cbda)]_n$ (**BUC-51**). Single-crystal X-ray crystallography analysis exhibited that **BUC-51** was constructed by $[Ag_2(bpy)_2(cbda)]$ chains linked via oxygen atoms from completely deprotonated $cbda^{2-}$ ligands. The *T*-shaped coordination geometries of the two crystallographically non-identical Ag(I) atoms were completed by two nitrogen atoms from two different bpy ligands and an oxygen atom from the completely depronted $cbda^{2-}$ ligand, in which Ag1-O and Ag2-O distances were 2.52(3) Å and 2.50(3) Å, respectively, much shorter than their van der Waals contact distance of 3.24 Å [22]. Finally, a 3D sandwich-like supramolecular framework was constructed from the infinite $[Ag_2(bpy)_2(cbda)]_n$ chains of **BUC-51** via π-π stacking interactions (Fig. 1a) [23].

$[Ag_3(bpy)_3(cpda)]\cdot(NO_3)\cdot 9H_2O$ (**BUC-52**) was made up of three infinite 1D $[Ag(bpy)]_n^{n+}$ chains, in which $[Ag1(bpy)]_n^{n+}$ and $[Ag2(bpy)]_n^{n+}$ was linked into double chain by a COO^- group from the completely deprotonated $cpda^{2-}$, while $[Ag3(bpy)]_n^{n+}$ chain was parallel to the above-stated double chain, as illustrated in Fig. 1b. There were three crystallographically non-identical Ag(I) atoms with different geometries in the crystal structure of **BUC-52**. The Ag1 atom, was four-coordinated by two nitrogen atoms from two different bpy ligands, and two oxygen atoms from the $cpda^{2-}$ ligand (Ag(1)*cdots*O(1) 2.650 Å and Ag(1)*cdots*O(2) 2.637 Å). The Ag2 atom, in *T*-shaped coordination geometry, was joined by two nitrogen atoms from two different bpy ligands and one oxygen atom from an oxygen atom from the same $cpda^{2-}$ linking Ag1. While the Ag3 atom was coordinated in a linear coordination geometry by two nitrogen atoms from two bpy ligands. Also, weak interactions between Ag3 atoms and the oxygen atoms from the adjacent lattice water molecules could be found, in which the Ag*cdots*O distances (2.732 Å) were longer than the genuine Ag-O distance [24]. Finally, the three types of infinite 1D $[Ag(bpy)]_n^{n+}$ chains were joined into 3D sandwich-like framework via hydrogen-bonding interactions, Ag*cdots*Ag interactions and Ag*cdots*N interactions (Tables S1–S3).

Both **BUC-51** and **BUC-52** stable in air and water, and they are insoluble in water and common organic solvents. The TGA results revealed that both these two CPs are thermally stable up to 266 °C and 245°, respectively, as shown in Fig. S2c. Furthermore, **BUC-51** and **BUC-52** also possess excellent photo-stabilities both in aqueous solution and dry solid state upon the visible light irradiation for 120 h and 72 h, respectively (Fig. S2a, b and d).

3.2. Adsorption experiments

In order to investigate the adsorption performance of **BUC-51** and **BUC-52** toward organic pollutants, adsorption experiments were carried out in batch system, in which some typical organic dyes like methyl orange (MO), congo red (CR), methylene blue (MB) and rhodamine B (RhB) were selected as target models. Both **BUC-51** and **BUC-52** exhibited poor uptake abilities to cationic MB and RhB, while they showed outstanding adsorption activities toward anionic MO and CR, as illustrated in Fig. S3. The maximum experimental adsorption capacities of **BUC-51** and **BUC-52** were 2606 mg/g & 1344 mg/g toward CR and 791 mg/g & 648 mg/g toward MO, respectively. It is worthy to note that the adsorption capacities of **BUC-51** and **BUC-52** toward CR and MO were much higher than most reported adsorbents, as shown in Tables S6 and S7.

To clarify the detailed adsorption behaviour, **BUC-51** and MO were selected as adsorbent and adsorbate, respectively. The corresponding adsorption kinetics, isotherm models and related thermodynamic parameters are calculated [17,25]. The pseudo-first-order model and the pseudo-second-order model had been often used to describe the adsorption kinetics processes. The calculated k_1 and k_2 values and their corresponding linear regression correlation coefficient (R^2) values of the above-stated two models are shown in Table S8. The obtained R^2 values for the pseudo-second-order model were above 0.99 at different concentrations, implying the pseudo-second-order model was more suitable to describe the related adsorption behaviour. A good agreement with pseudo-second-order model was also confirmed by similar values between the calculated q_e ones and the experimental ones, as listed in Table S8.

It is necessary to clarify the equilibrium isotherms, hence, the equilibrium data of MO adsorbing onto **BUC-51** at different temperatures of 288 K, 293 K, 298 K, 303 K and 308 K were fitted with Langmuir, Freundlich and Dubinin–Radushkevich (D-R), respectively. The higher coefficients R^2 ranging from 0.979 to 0.999 of Langmuir equations showed that Langmuir isotherm model preferred to describe the adsorption process [26], as listed in Table S9. As well, the q_{max} values obtained from Langmuir model decreased with the increasing temperature, suggesting that the adsorption was favourable at higher temperature and the process was endothermic.

As listed in Table S10, the values of ΔG^0 decreased from −28.16 to −33.80 kJ/mol with the increase of temperature from 288 K to 308 K, implying that the adsorption process became more favourable at higher temperatures [27]. The negative ΔG^0 values suggested that the sorption process may be controlled by mainly physical sorption and partially chemical sorption [17]. The positive value of ΔH^0 (54.66 kJ/mol) indicated that the adsorption reaction between MO and **BUC-51** is endothermic, evidenced by the increase of adsorption capacity with temperature [28]. The positive ΔS^0 value (286 J/(mol·K)) demonstrated the increased randomness happens at the solid-solution interface during the affinity of MO onto **BUC-51** [29].

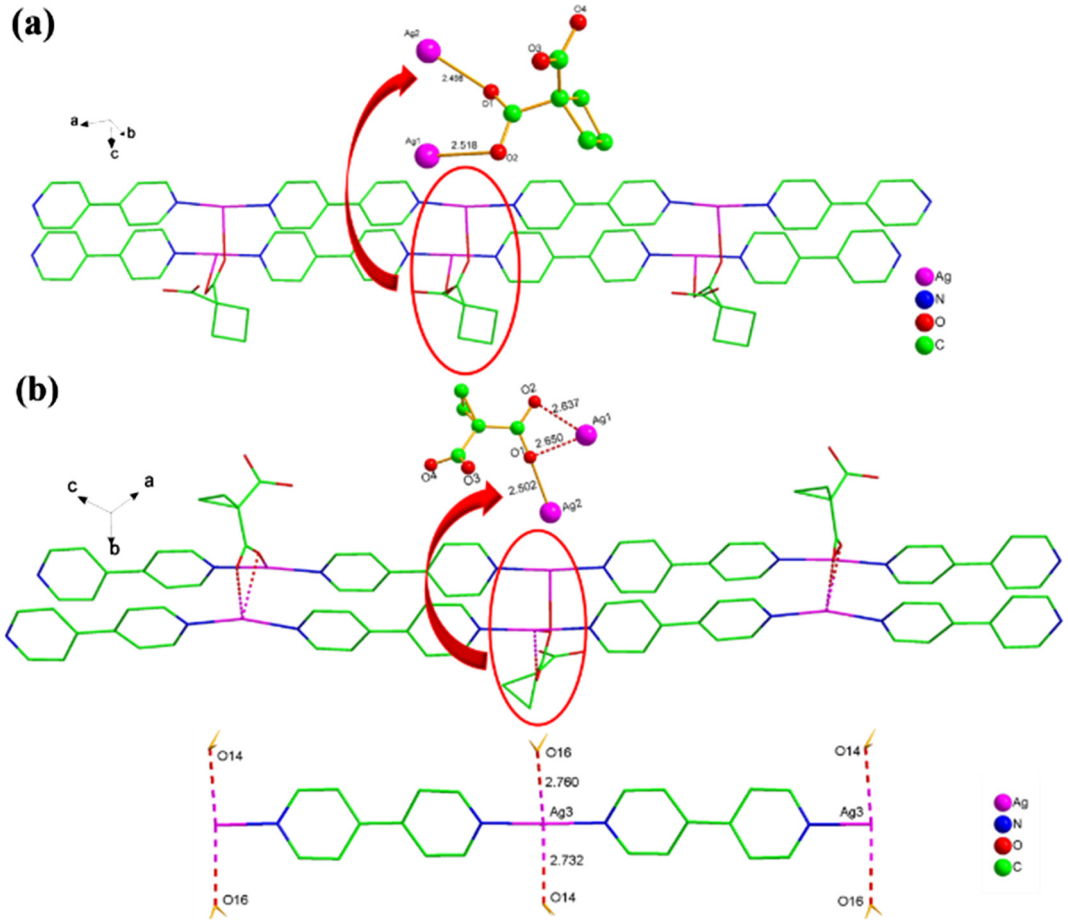

Fig. 1. (a) The 1D infinite $[Ag_2(bpy)_2(cbda)]_n$ chain in **BUC-51**. (b) The Ag-Ag and Ag-O interactions between neighbouring 1D infinite $[Ag_3(bpy)_3(cpda)]_n^{n+}$ chains in **BUC-52**.

3.3. FTIR and XPS analyses

In order to illustrate the adsorption mechanism, FTIR and XPS were used to study the adsorption process. Before adsorption, the peak observed in the range of 3050–3600 cm^{-1} was due to the presence of —OH groups in the **BUC-51**. The peak at 1487 cm^{-1} can be contribute to the stretching of —CH groups (V and δ). The peaks in region of 1590–1620 cm^{-1} were due to the stretching vibration of C—N group, and the peaks ranging from 1636 to 1410 cm^{-1} were ascribed to the skeletal vibration of pyridyl rings. The absorption peaks of symmetrical and asymmetrical stretching vibration of C—O are at 1226 cm^{-1} and 1314 cm^{-1}, respectively.

After adsorption, some changes were observed in the FTIR spectra as a result of the interactions between the MO dye and **BUC-51**. The peak in the range of 1367 cm^{-1} was due to the stretching of —S═O group, indicating successful adsorption of MO dye onto the **BUC-51** surface [30]. Further, the peak intensity of C—N at 1601 cm^{-1} was increased after the adsorption of MO dyes. Moreover, the weak peak at 1040 cm^{-1} corresponded to the —N═N— stretching vibration in Fig. 2a [31].

The XPS spectra of O, Ag and S of MO/CR/BB-1@**BUC-51** were tested to further provide the information of the interactions between **BUC-51** and different adsorbates (Fig. 2b). Meanwhile, the elemental mapping obtained from SEM revealed the existence of S (the characteristics element of MO) in **BUC-51** after adsorbing MO, besides of Ag, C, N and O elements in as-prepared **BUC-51** (Fig. 3).

3.4. Adsorption mechanism analysis

To test the adsorption performances to different organic dyes, series dyes were selected to contact with **BUC-51**. As listed in Table S11, **BUC-51** preferred to suck fourteen anionic organic dyes and one neutral organic dyes with sulfonic groups, witnessed by the corresponding adsorption capacities ranging from 2606 mg/g toward CR to 489 mg/g toward acid chrome blue K (ACBK) (Fig. 4). It was deemed that the interactions between Ag(I) and oxygen atom from —SO_3 group contributed to the excellent adsorption performance of **BUC-51** toward the dyes with sulfonic groups. In general, Ag(I) is found in a wide range of coordination environments: linear, trigonal, tetrahedral, square-planar, square-pyramidal and octahedral [32]. While, all the Ag(I) centers in **BUC-51** adopted three-coordinated trigonal coordination environments, implying that the uncoordinated sites might be potentially occupied by oxygen atoms from —SO_3 in the selected dyes via weak Ag*ldots*O interactions [32]. The interaction between Ag^+ and —SO_3 can be verified by the identical mole number of Ag^+ in **BUC-51** and —SO_3 group(s) in the related organic dyes as listed in Table S12, i.e. the experimental adsorption capacities of **BUC-51** toward corresponding dyes were nearly equal to the calculated ones (except for CR and AF). Taking the adsorption of MO and CR onto **BUC-51** as example, the strong XPS spectra signals of S element (the characteristics element of MO & CR) with binding energy of 168.14 eV (Fig. 2c) could be observed. The XPS spectra showed that the interaction between MO and **BUC-51** led to Ag(I) peaks' slight shifted from 368.02 eV (3d 5/2) and 374.01 eV (3d 3/2) in

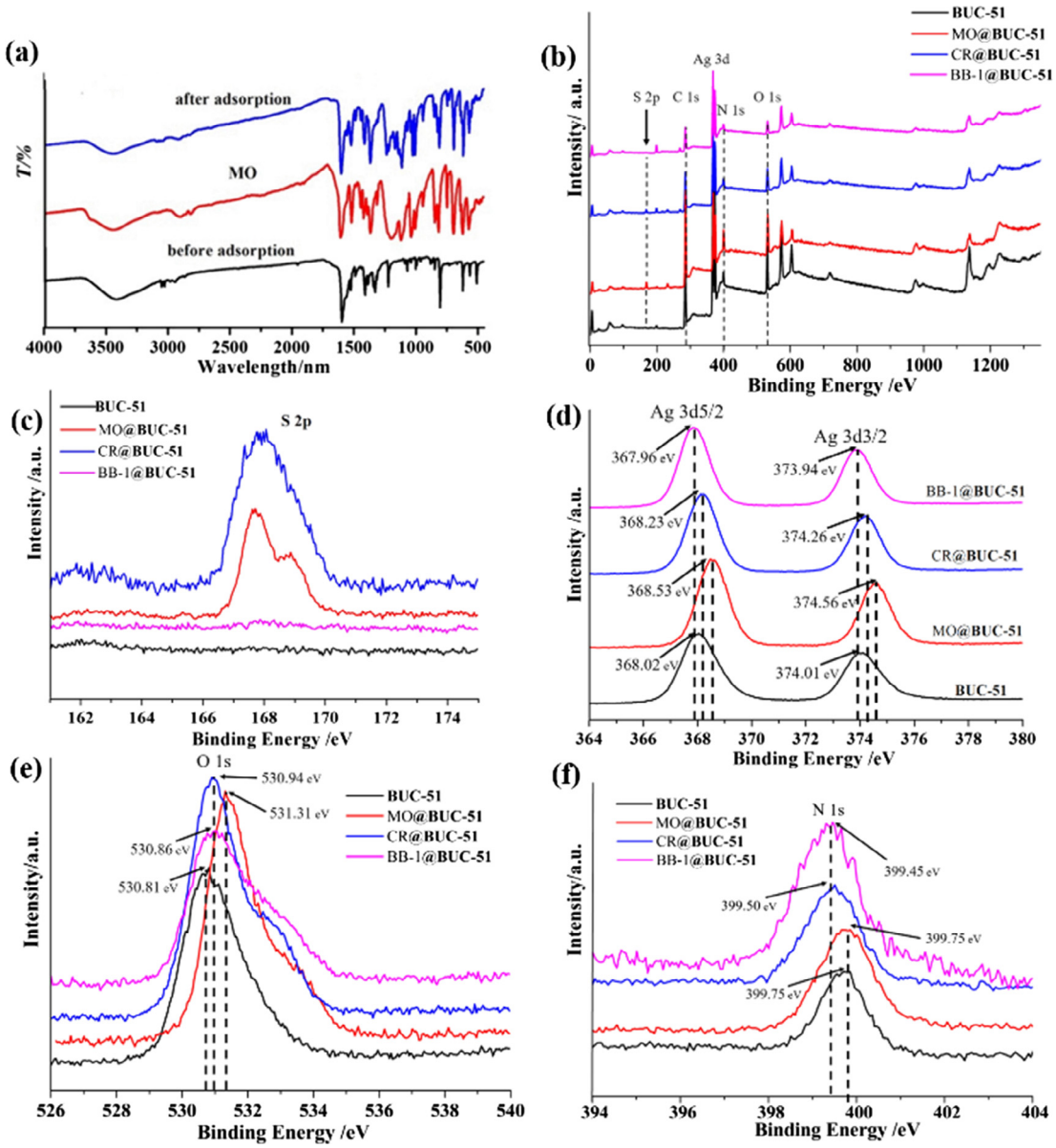

Fig. 2. (a) FTIR spectra of as-synthesized **BUC-51**, MO dye, **BUC-51** after absorbing MO. (b) XPS wide scanning spectra of **BUC-51** before and after adsorption. (c) XPS spectra for S 2p in **BUC-51** before and after adsorbing different dyes. (d) XPS spectra for Ag 3d in **BUC-51** before and after adsorbing different dyes. (e) XPS spectra for O 1s in **BUC-51** before and after adsorbing different dyes. (f) XPS spectra for N 1s in **BUC-51** before and after adsorbing different dyes.

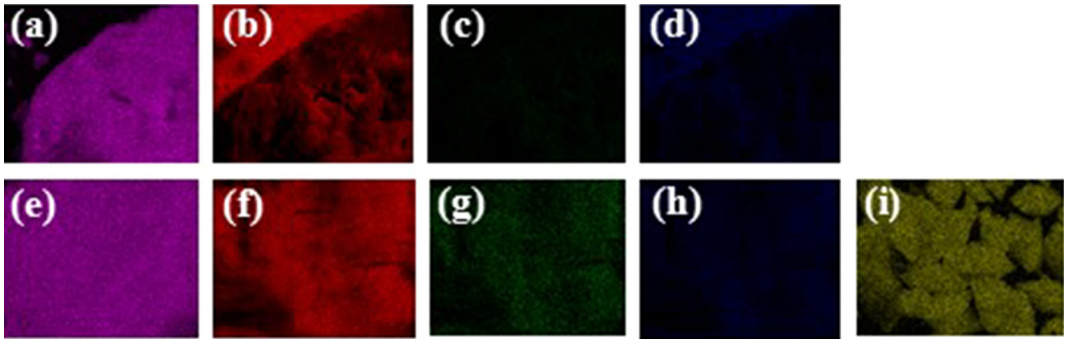

Fig. 3. (**a**)–(**d**) Ag, N, O, and C elemental mapping of **BUC-51**, (**e**)–(**j**) Ag, N, O, C and S elemental mapping of **BUC-51** after adsorption.

original **BUC-51** to 368.53 eV and 374.56 eV in MO**@BUC-51** (Fig. 2d), along with that O 1s peak shifted from 530.81 eV before adsorption to 531.31 eV after adsorption (Fig. 2e), which could be assigned to weak Ag*cdots*O interactions [33]. Additionally, the presence of —NH_2 groups in some dye molecules like CR and BB-1 could enhance the formation of hydrogen-bonding interactions

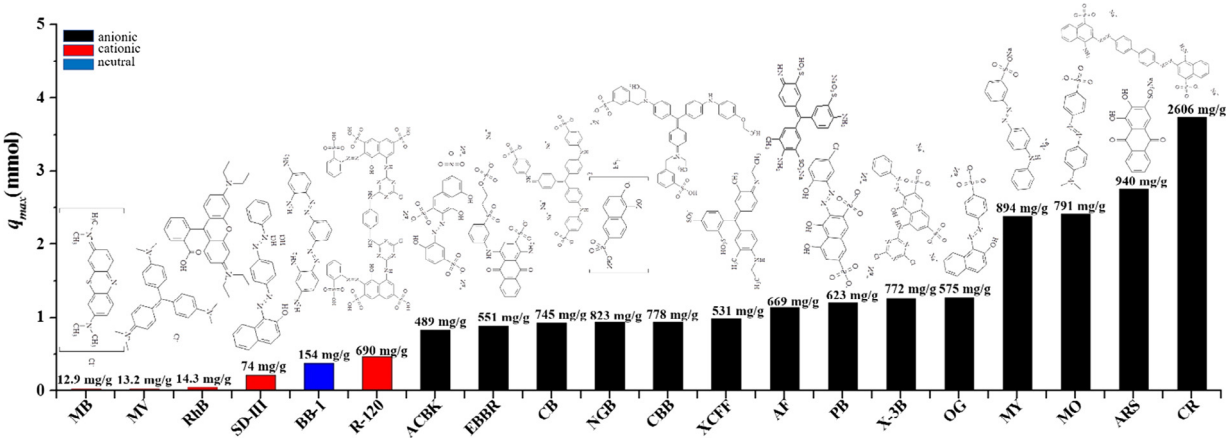

Fig. 4. The adsorption performance of **BUC-51** towards 20 dyes (The numbers above the column represented the adsorption capacity towards different dyes with unit of mg/g). methylene blue (MB), methyl violet (MV), rhodamine B (RhB), sudan III (SD-III), basic brown 1 (BB-1), procion red H-E3B (R120), acid chrome blue K (ACBK), eriochrome blue black R (EBBR), cotton blue (CB), naphthol green B (NGB), coomassie brilliant blue R-250 (CBB), xylene cyanol FF (XCFF), acid Fuchsin (AF), plasmocorinth B (PB), reactive red 2 (X-3B), acid orange G (OG), metanil yellow (MY), methyl orange (MO), alizarin red S (ARS), congo red (CR).

with **BUC-51** as adsorbent (Fig. 2f). After the adsorption of CR and BB-1, the peak of nitrogen atom in —NH_2 shifted to a lower binding energy of 399.45 eV, implying the formation of hydrogen bonding interactions [34], which might lead to ultra-high adsorption capacity of 2606 mg/g toward MO, much higher than the calculated value of 1309 mg/g. In addition, the weak π–π stacking interactions between the pyridine rings of **BUC-51** and the aromatic rings of CR might contribute its remarkable adsorption performance toward CR [36,37]. The possible interaction mechanism between organic dyes like CR and **BUC-51** was proposed in Fig. 5.

Considering that **BUC-51** surface displayed positive with Zeta potential ranging from 0 mV to 32.24 mV at the pH range of 2.5–7.8 (Fig. S4), **BUC-51** was inhospitable to cationic dyes like MB and RhB whose initial pH values before adsorption were under 7.0. However, it can absorb cationic basic brown 1 (BB-1) with adsorption capacity of 154 mg/g, further confirming the contribution of hydrogen-bonding interactions between —NH_2 groups in BB-1 and the organic linkers in **BUC-51** [35].

3.5. SPE column test

Based on the **BUC-51**'s preferential uptake toward anionic dyes with —SO_3 groups and inert to most cationic dyes, solid phase extraction (SPE) was adopted to test the separation ability to dyes matrix like MO (10 mg/L)/MB (10 mg/L) mixture, in which the Agilent Bond Elut C18 in commercially available SPE column was replaced by 1.0 g **BUC-51** with particle size of about 0.1 mm. The MO/MB mixture was pumped through the SPE column via automatic vacuum with the flow rate of 15 mL/min (Fig. 6 and Video 1). The MO was retained in **BUC-51**, whereas the MB passed through the SPE column completely and quickly, indicating that **BUC-51** could rapidly and efficiently separate MO and MB from their mixture.

Video 1.

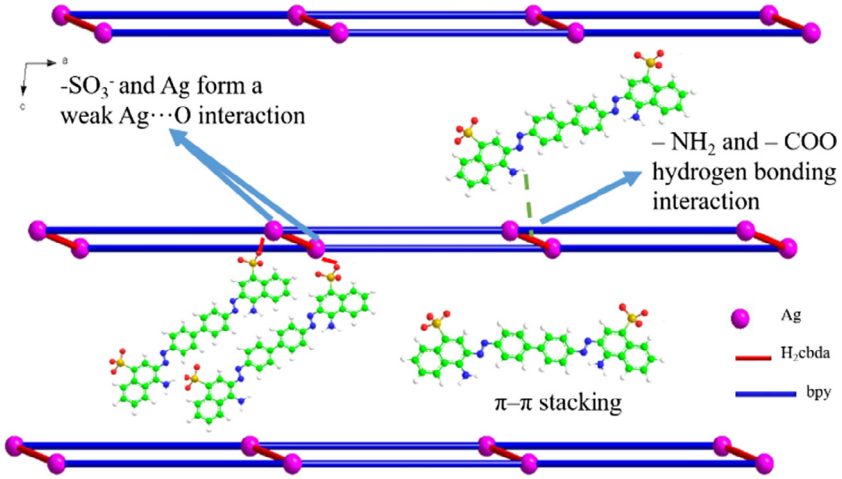

Fig. 5. The possible adsorption mechanism between **BUC-51** and CR.

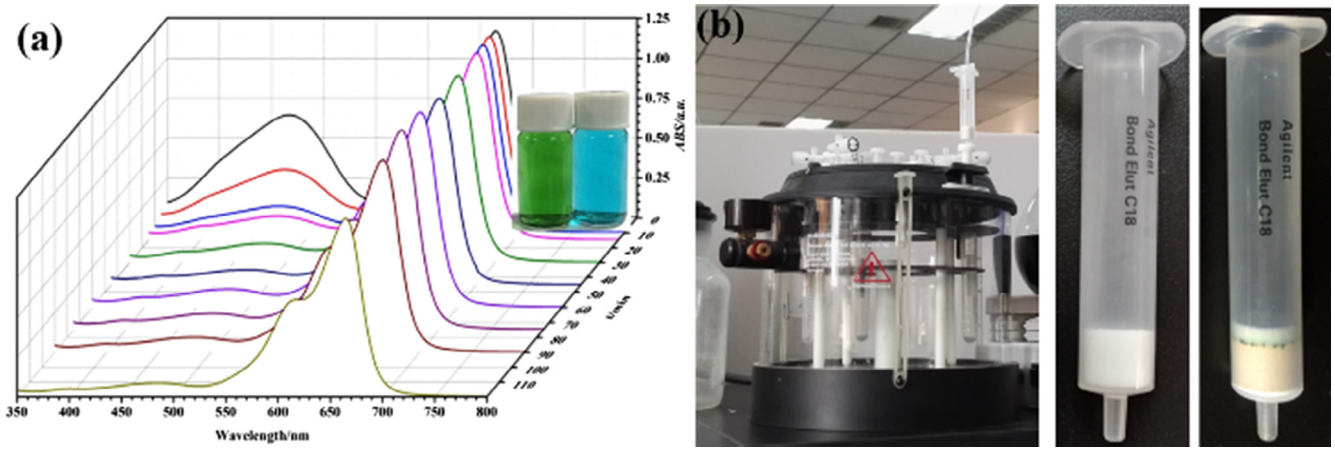

Fig. 6. (a) UV–Vis spectral changes of the dye mixtures of MO and MB. (b) The picture of SPE setup, in which the original packing material C18 was replaced by **BUC-51**.

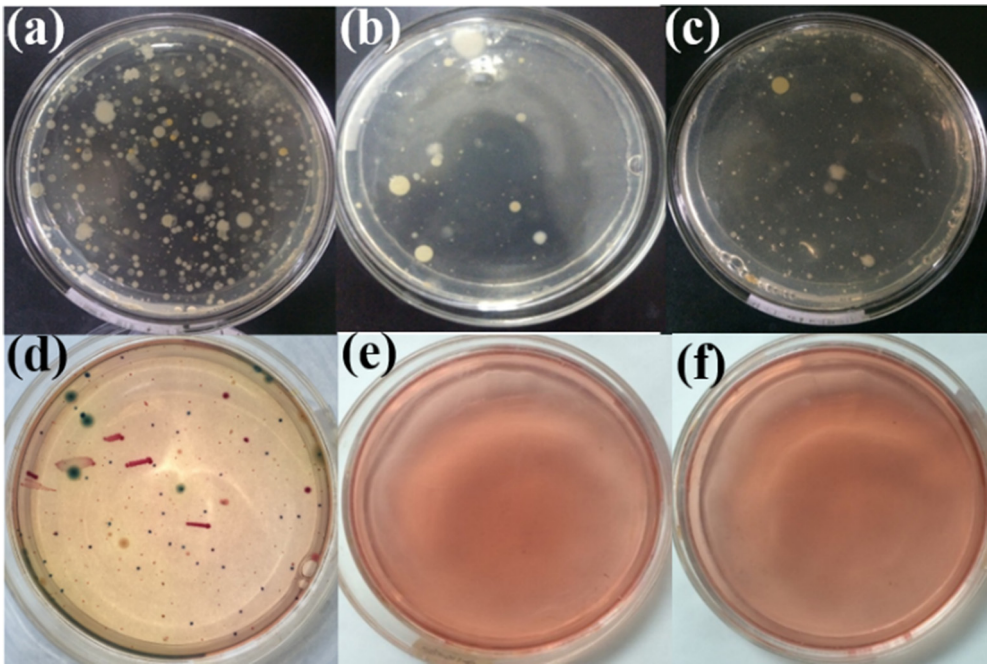

Fig. 7. Agar plate diffusion experiment to estimate antibacterial activity of **BUC-51** and **BUC-52** onto surface layer of lake water. ((a) with the absence of **BUC-51** and **BUC-52**. (b), (e) with the presence of **BUC-51**. (c), (f) with the presence of **BUC-52**. Incubation conditions, 310 K, 24 h).

3.6. Antibacterial activities

Surface water samples collected from Minghu Lake at BUCEA campus were used to test the antibacterial abilities of **BUC-51** and **BUC-52**, following agar plate diffusion assay method [20] (Experimental details can be found in ESI†). Two micrograms **BUC-51** and **BUC-52** powders with particle size less than 0.1 mm were added to 200 mL surface water samples, respectively. After 4 h cultivation, the supernatant was vaccinated onto an Agar plate to observe the growth status of bacterial colonies. The number of bacterial colonies was 8740 CFU/mL in the absence of **BUC-52** and **BUC-51**, which decreased to 103 CFU/mL and 169 CFU/mL in the presence of **BUC-51** and **BUC-52**, respectively, as illustrated in the Fig. 7. In detail, both **BUC-52** and **BUC-51** could efficiently inhibit the growth of ATCC 23355 Enterobacter cloacae, ATCC 14028 salmonella, ATCC 25922 Enterobacter aerogenes, ATCC 35029 citrobacter and so on, as listed in Fig. 7 and Table S13, indicating that both **BUC-51** and **BUC-52** exhibited remarkable antibacterial properties.

To evaluate the antibacterial performances of **BUC-51** and **BUC-52**, gram-negative *E. coli* was selected as model microorganism to conduct series experiments. The minimum inhibitory concentration (MICs) of **BUC-51** and **BUC-52** were determined by using an optical density methods [38]. The MICs of these two CPs against *E. coli* were in the range of 10–15 and 15–20 ppm (Fig. S5), respectively, which revealed that **BUC-51** and **BUC-52** exhibited higher antibacterial activities than most of commonly used silver-based compounds and chemical disinfectants reported previously [3,39,40].

The time-dependent antimicrobial activities of **BUC-51** and **BUC-52** in different concentrations against *E. coli* were illustrated in Fig. 8. The obvious inhibitory effect of these two CPs versus *E. coli* started at less than 20 ppm for a long period of time (48 h) (Fig. S6). The previous researches revealed that Ag nano-particles

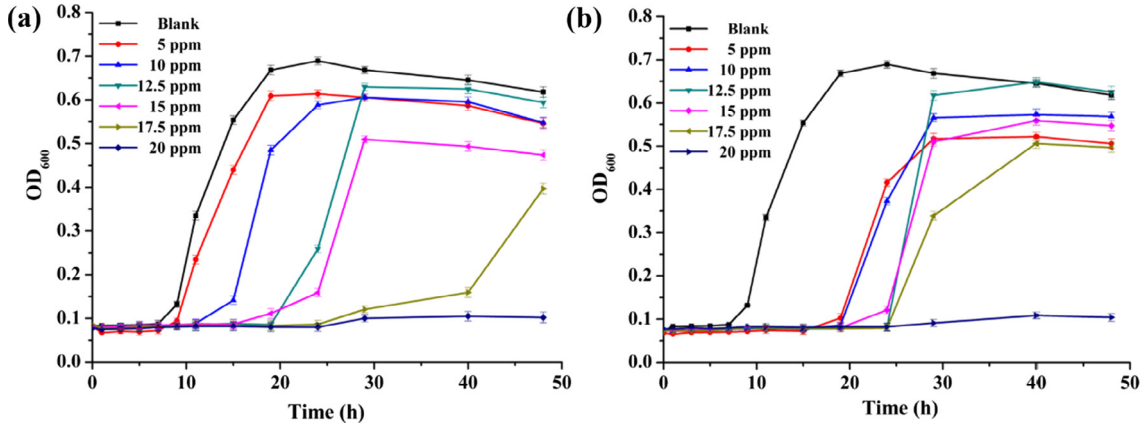

Fig. 8. Growth curves of *E. coli* in different concentrations (5–20 ppm) of **BUC-51** (a) and **BUC-52** (b).

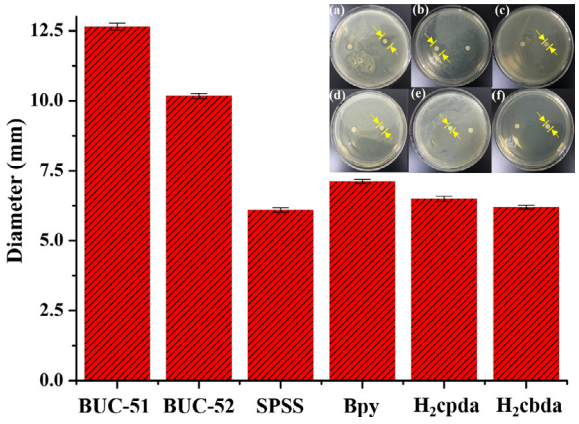

Fig. 9. Images and diameters of inhibition zones for **BUC-51** (a), **BUC-52** (b), SPSS (c), bpy (d), H_2cbda (e) and H_2cpda (f) against *E. coli*.

demonstrated nearly no impact on *E. coli* below the concentration of 40 ppm [41], demonstrating that both **BUC-51** and **BUC-52** showed efficient and long-lasting antibacterial activities at relatively low concentration. Additionally, the diameters of inhibition zones of **BUC-51** (12.58 mm), **BUC-52** (10.46 mm), stroke-physiological saline solution (SPSS, 6 mm) and free ligands (7.12 mm for bpy, 6.3 mm for H_2cpda, and 6.1 mm for H_2cbda) confirmed superior antimicrobial properties of these two Ag-based CPs (Fig. 9).

3.7. Antibacterial mechanism

It is generally known that the antibacterial activities of Ag-based materials resulted from the release of Ag^+ ions [41,42]. The Ag^+ release abilities of **BUC-51** and **BUC-52** were determined by ICP-OES, and the results revealed that the Ag^+ release rate increased significantly during the first 16 h, and then they retained at a stable level (average released Ag^+ concentration being 37.21 ppm and 35.24 ppm for **BUC-51** and **BUC-52**, respectively) for 5 d, as illustrated in Fig. 10. Compared with other Ag-based CPs reported previously [43], **BUC-51** and **BUC-52** exhibited moderate Ag^+ ion release rate, indicating that both CPs could provide steady and prolonged release of Ag^+ ions to ensure their excellent antibacterial performances.

To understand the antibacterial process of these two Ag-based CPs against *E. coli*, the morphological changes of bacteria cells were observed by Transmission electron microscope (TEM) and scanning electron microscope (SEM), as illustrated in Fig. 11. Intact *E. coli* in Fig. 11a and c had distinct outer membranes, suggesting that the bacteria cell structures were well-preserved even under high vacuum and energy electron beam. However, when the *E. coli* bacteria were exposed to **BUC-51**, they lost the cellular cohesion with their outer membranes being seriously destroyed, leading to the bacteria's cytoplasm outflow and then death (Fig. 11c and d).

Based on our experimental results, a possible antibacterial mechanism of these two silver-based CPs (taking **BUC-51** as example) was proposed as showed in Fig. 12. The **BUC-51** particles

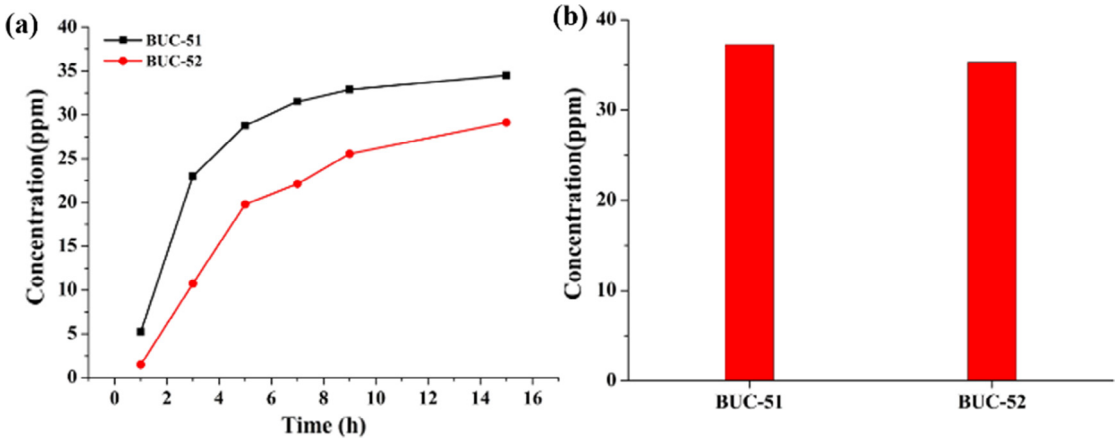

Fig. 10. (a) Concentrations of released Ag^+ from **BUC-51** and **BUC-52** aqueous solution and the average concentrations of Ag^+ in **BUC-51** and **BUC-52** aqueous solution within 5 d (b).

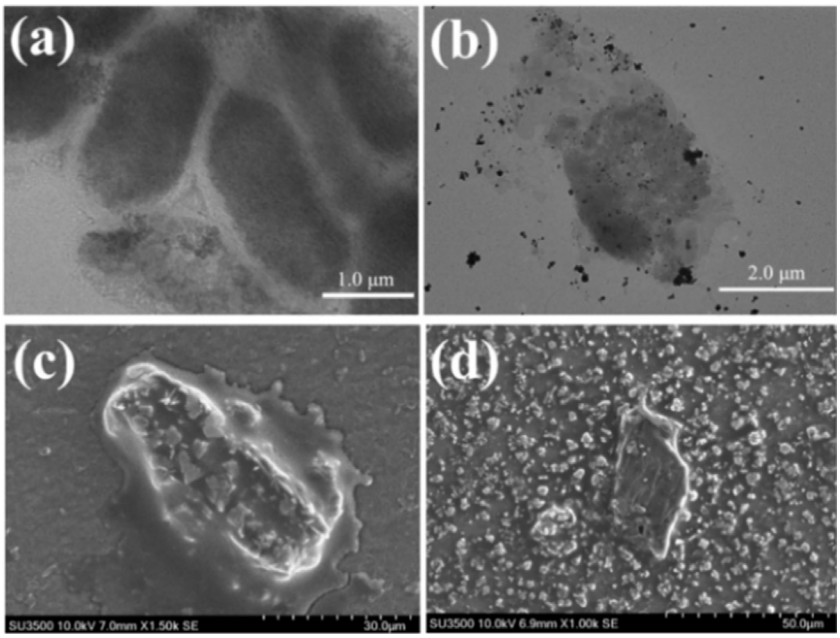

Fig. 11. TEM (a, b) and SEM (c, d) morphological images of cell structures: intact and damaged *E. coli* by **BUC-51** (1 h).

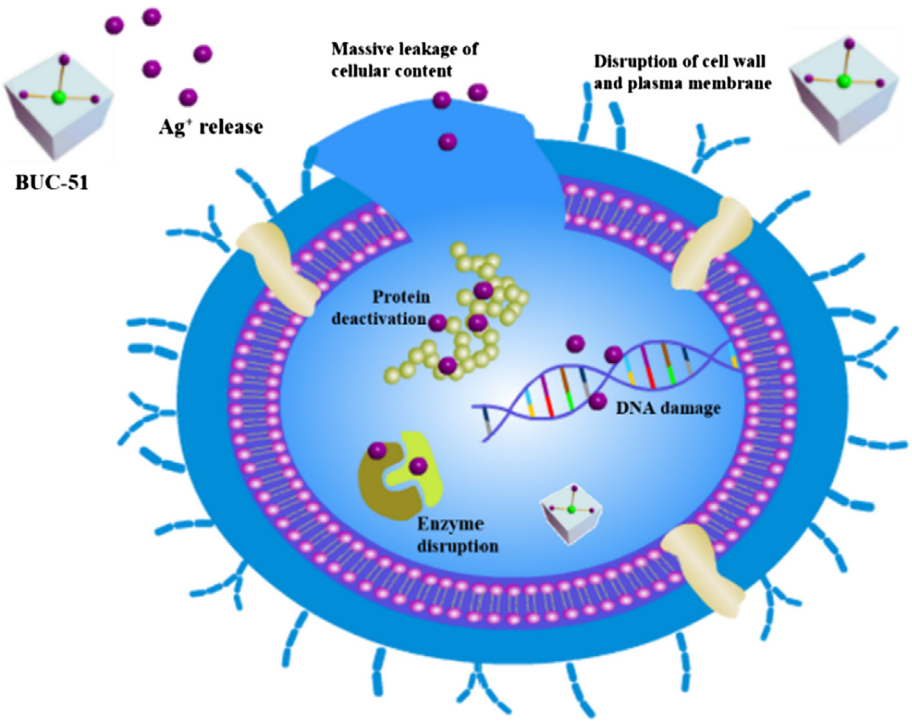

Fig. 12. Schematic representation of the bactericidal mechanism for Ag-based coordination polymers as disinfectants.

diffused into the E. *coli* bacteria surface, and released Ag^+ ions led to the ion balance being broken and the ion channels being destroyed [44,45]. Also, the fine particle of **BUC-51** can penetrate into the bacteria to destroy the cells by interaction with lipotropic acid or hydroxyl groups of peptidoglycan membranes and phosphate groups of phosphonolipid membranes [38,41,46]. Furthermore, the Ag^+ ions might interact with the thiol groups of proteins to disturb bacterial membrane's integrity and permeability [46,47]. Finally, with the rupture of the cell membrane, the outflow of cytoplasm caused the death of bacteria.

4. Conclusions

In all, $[Ag_2(bpy)_2(cbda)]$ (**BUC-51**) and $[Ag_3(bpy)_3(cpda)]\cdot(NO_3)\cdot 9H_2O$ (**BUC-52**) were synthesized from the reaction of Ag(I) salts with two similar dicarbolylic linkers 1,1-cyclopropanedicarboxylic acid (H_2cpda)/1,1-cyclobutane dicarboxylic acid (H_2cbda) and 4,4′-bipyridine (bpy) via slow evaporation method. Both these two CPs possessed 1D infinite chain-like structures, which exhibited good thermal stability, water stability and optical ability under UV–visible light. **BUC-51** preferred to adsorb 14 anionic organic dyes and one

neutral organic dyes with sulfonic groups, whose adsorption capacities ranged from 2606 mg/g to 489 mg/g. Furthermore, **BUC-51** was used to prepare a SPE column, which was used to efficiently separate different organic dyes from their mixture. The controlled slow-release of Ag^+ ions from **BUC-51** and **BUC-52** contributed to excellent antibacterial activities toward Gram-negative bacteria *E. coli*. with lower MICs and wider inhibition zones. Compared with traditional adsorbent such as activated carbon, which has higher adsorption ability of organic pollutants, and other CPs in wastewater treatment, the Ag-CPs has good antibacterial effect, which can prevent the adsorbent surface adheres to the biofilm and keep adsorption effect. As well, the possible mechanisms of outstanding adsorption performances and excellent antibacterial abilities were proposed. Considering ultrahigh adsorption capacities, efficient separation ability and excellent antibacterial effect of these two CPs, it could be believed that more similar Ag-based CPs can be prepared to help the environment. Further researches are planned to conduct the efficient adsorption toward PPCPs (Pazufloxacin Mesylate and pefloxacin mesylate with $-SO_3^-$, sulfamethoxazole with $-NH_2$) and heavy metals with different electric charge (cationic Pb^{2+}, Cd^{2+} and anionic $Cr_2O_7^{2-}$).

Acknowledgements

The authors acknowledge the financial support from National Natural Science Foundation of China (51578034), the Beijing Natural Science Foundation & Scientific Research Key Program of Beijing Municipal Commission of Education (KZ201410016018), Beijing Talent Project (2016023), Project of Construction of Innovative Teams and Teacher Career Development for Universities and Colleges Under Beijing Municipality (IDHT20170508).

Appendix A. Supplementary material

Supplementary data associated with this article can be found, in the online version, at https://doi.org/10.1016/j.jcis.2017.10.099.

References

[1] J. Lee, O.K. Farha, J. Roberts, K.A. Scheidt, S.T. Nguyen, J.T. Hupp, Chem. Soc. Rev. 38 (2009) 1450.
[2] C.C. Wang, J.R. Li, X.L. Lv, Y.Q. Zhang, G. Guo, Energy Environ. Sci. 7 (2014) 2831.
[3] G. Wyszogrodzka, B. Marszałek, B. Gil, P. Dorożyński, Drug Discov. Today 21 (2016) 1009.
[4] J.-R. Li, R.J. Kuppler, H.-C. Zhou, Chem. Soc. Rev. 38 (2009) 1477.
[5] E.M. Dias, C. Petit, J. Mater. Chem. A 3 (2015) 22484.
[6] B. Gole, A.K. Bar, P.S. Mukherjee, Chem. Commun. 47 (2011) 12137.
[7] W.J. Li, J. Lu, S.Y. Gao, Q.H. Li, R. Cao, J. Mater. Chem. A 2 (2014) 19473.
[8] L. Sorace, C. Benelli, D. Gatteschi, Chem. Soc. Rev. 40 (2011) 3092.
[9] K.M. Taylor-Pashow, J.D. Rocca, Z. Xie, S. Tran, W. Lin, J. Am. Chem. Soc. 131 (2009) 14261.
[10] Y. He, J. Shang, Q. Gu, G. Li, J. Li, R. Singh, P. Xiao, P.A. Webley, Chem. Commun. 51 (2015) 14716.
[11] S. Kitagawa, R. Matsuda, Coord. Chem. Rev. 251 (2007) 2490.
[12] S. Sorribas, B. Zornoza, C. Téllez, J. Coronas, Chem. Commun. 48 (2012) 9388.
[13] Y.-C. He, J. Yang, Y.-Y. Liu, J.-F. Ma, Inorganic Chem. 53 (2014) 7527.
[14] X.-D. Du, C.-C. Wang, J. Zhong, J.-G. Liu, Y.-X. Li, P. Wang, J. Environm. Chem. Eng. 5 (2017) 1866.
[15] H.-N. Wang, F.-H. Liu, X.-L. Wang, K.-Z. Shao, Z.-M. Su, J. Mater. Chem. A 1 (2013) 13060.
[16] J. Huo, J. Aguilera-Sigalat, S. El-Hankari, D. Bradshaw, Chem. Sci. 6 (2015) 1938.
[17] J.-J. Li, C.-C. Wang, H. Fu, J.-R. Cui, P. Xu, J. Guo, J.-R. Li, Dalton Trans. (2017) 10197.
[18] X. Lu, J. Ye, Y. Sun, R.F. Bogale, L. Zhao, P. Tian, G. Ning, Dalton Trans. 43 (2014) 10104.
[19] R. Kumar, H. Münstedt, Biomaterials 26 (2005) 2081.
[20] K. Fiebelkorn, S. Crawford, M. McElmeel, J. Jorgensen, J. Clin. Microbiol. 41 (2003) 4740.
[21] A. Bauer, W. Kirby, J.C. Sherris, M. Turck, Am. J. Clin. Pathol. 45 (1966) 493.
[22] J.C. Jin, Y.Y. Wang, W.H. Zhang, A.S. Lermontov, L. Ekh, Q.Z. Shi, Dalton Trans. 46 (2009) 10181.
[23] Z. Hasan, S.H. Jhung, J. Hazard. Mater. 283 (2015) 329.
[24] A.G. Young, L.R. Hanton, Coord. Chem. Rev. 252 (2008) 1346.
[25] N.A. Khan, J.W. Jun, J.H. Jeong, S.H. Jhung, Chem. Commun. 47 (2011) 1306.
[26] E. Haque, V. Lo, A. Minett, A. Harris, T. Church, J. Mater. Chem. A 2 (2013) 193.
[27] A. Zaki, M. El-Sheikh, J. Evans, S. El-Safty, J. Colloid Interface Sci. 221 (2000) 58.
[28] A. Mittal, D. Jhare, J. Mittal, J. Mol. Liq. 179 (2013) 133.
[29] A.B. Karim, B. Mounir, M. Hachkar, M. Bakasse, A. Yaacoubi, J. Hazard. Mater. 168 (2009) 304.
[30] X. Liang, Y. Xiong, S. Tian, C. He, Q. Su, Z. Wen, Chem. Eng. J. 265 (2015) 157.
[31] H. Hou, R. Zhou, P. Wu, L. Wu, Chem. Eng. J. s 211–212 (2012) 336.
[32] A.Y. Robin, K.M. Fromm, Coord. Chem. Rev. 250 (2006) 2127.
[33] V.I. Bukhtiyarov, A.I. Boronin, I.P. Prosvirin, V.I. Savchenko, J. Catal. 150 (1994) 268.
[34] J.S. Stevens, S.J. Byard, C.C. Seaton, G. Sadiq, R.J. Davey, S.L. Schroeder, Phys. Chem. Chem. Phys. 16 (2014) 1150.
[35] X.-D. Du, C.-C. Wang, J.-G. Liu, X.-D. Zhao, J. Zhong, Y.-X. Li, J. Li, P. Wang, J. Colloid Interface Sci. 506 (2017) 437.
[36] T. Shen, J. Luo, S. Zhang, X. Luo, J. Environm. Chem. Eng. 3 (2014) 1372.
[37] J. Ma, F. Yu, L. Zhou, L. Jin, M. Yang, J. Luan, Y. Tang, H. Fan, Z. Yuan, J. Chen, Acs Appl. Mater. Interfaces 4 (2012) 5749.
[38] M. Yamanaka, K. Hara, J. Kudo, Appl. Environ. Microbiol. 71 (2005) 7589.
[39] K. Chamakura, R. Perez-Ballestero, Z. Luo, S. Bashir, J. Liu, Colloids Surf., B 84 (2011) 88.
[40] N.C. Kasuga, A. Sugie, K. Nomiya, Dalton Trans. 21 (2004) 3732.
[41] X. Lu, J. Ye, D. Zhang, R. Xie, R.F. Bogale, Y. Sun, L. Zhao, Q. Zhao, G. Ning, J. Inorg. Biochem. 138 (2014) 114.
[42] W. Zhang, Y. Yao, N. Sullivan, Y. Chen, Environ. Sci. Technol. 45 (2011) 4422.
[43] Y. Liu, X. Xu, Q. Xia, G. Yuan, Q. He, Y. Cui, Chem. Commun. 46 (2010) 2608.
[44] E. Kopera, T. Schwerdtle, A. Hartwig, W. Bal, Chem. Res. Toxicol. 17 (2004) 1452.
[45] L. Thornton, V. Dixit, L.O. Assad, T.P. Ribeiro, D.D. Queiroz, A. Kellett, A. Casey, J. Colleran, M.D. Pereira, G. Rochford, J. Inorg. Biochem. 159 (2016) 120.
[46] S. Medici, M. Peana, G. Crisponi, V.M. Nurchi, J.I. Lachowicz, M. Remelli, M.A. Zoroddu, Coord. Chem. Rev. 327–328 (2016) 349.
[47] Y. Matsumura, K. Yoshikata, S. Kunisaki, T. Tsuchido, Appl. Environ. Microbiol. 69 (2003) 4278.